BIOCHEMISTRY
including biophysical chemistry & molecular biology

ARTICLE

pubs.acs.org/biochemistry

Computational Modeling of Substrate Specificity and Catalysis of the β-Secretase (BACE1) Enzyme

Arghya Barman,[†] Stephan Schürer,[‡] and Rajeev Prabhakar*[,†]

[†]Department of Chemistry, University of Miami, 1301 Memorial Drive, Coral Gables, Florida 33146, United States

[‡]Department of Molecular and Cellular Pharmacology, Miller School of Medicine and Center for Computational Science, University of Miami, Miami, Florida 33136, United States

Supporting Information

ABSTRACT: In this combined MD simulation and DFT study, interactions of the wild-type (WT) amyloid precursor protein (APP) and its Swedish variant (SW), Lys670 → Asn and Met671 → Leu, with the beta-secretase (BACE1) enzyme and their cleavage mechanisms have been investigated. BACE1 catalyzes the rate-limiting step in the generation of 40−42 amino acid long Alzheimer amyloid beta (Aβ) peptides. All key structural parameters such as position of the flap, volume of the active site, electrostatic binding energy, structures, and positions of the inserts A, D, and F and 10s loop obtained from the MD simulations show that, in comparison to the WT-substrate, BACE1 exhibits greater affinity for the SW-substrate and orients it in a more reactive conformation. The enzyme−substrate models derived from the MD simulations were further utilized to investigate the general acid/base mechanism used by BACE1 to hydrolytically cleave these substrates. This mechanism proceeds through the following two steps: (1) formation of the gem-diol intermediate and (2) cleavage of the peptide bond. For the WT-substrate, the overall barrier of 22.4 kcal/mol for formation of the gem-diol intermediate is 3.3 kcal/mol higher than for the SW-substrate (19.1 kcal/mol). This process is found to be the rate-limiting in the entire mechanism. The computed barrier is in agreement with the measured barrier of ca. 18.00 kcal/mol for the WT-substrate and supports the experimental observation that the cleavage of the SW-substrate is 60 times more efficient than the WT-substrate.

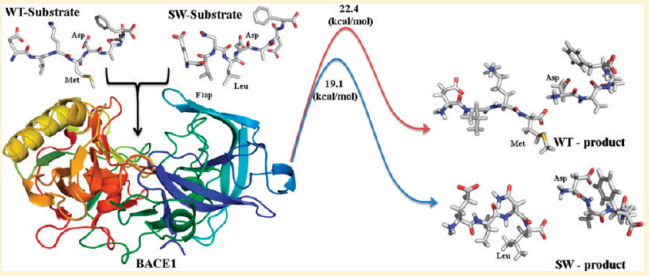

Aspartyl proteases constitute a ubiquitous family of enzymes that is present in vertebrates, fungi, plants, and retroviruses.[1−4] On the basis of their structural characteristics, these enzymes are divided into the following two classes: (I) pepsin-like (renin, cathepsin D, chymosin, and memapsin 2 or beta secretase, etc.) and (II) retroviral (HIV protease and malaria protease).[5,6] Despite the structural differences, the pepsin-like and retroviral protease families are evolutionary related, and almost all their members contain a catalytic Asp dyad at the active site covered over by an antiparallel hairpin loop known as flap.[7,8] During the catalytic cycle, the flap must open to allow the entrance of the substrate into the active site cleft and steer it toward the catalytic Asp dyad to attain a reactive conformation. In this conformation the specific peptide bond(s) of the substrate is hydrolytically cleaved.

In the pepsin-like aspartic proteases, mechanisms of flap closing and catalysis are of great significance due to their involvement in human diseases such as Alzheimer's disease (AD).[9] AD is characterized by the deposition of extracellular plaques inside the brain.[10] The major components of these plaques are 40−42 amino acid residues containing amyloid beta peptides (Aβ40 or Aβ42).[11−13] β-Secretase (BACE1) catalyzes the rate-limiting step of the Aβ generation by cleaving the Met671−Asp672 peptide bond of APP (isoform 770, identifier P050677) at the extracellular space.[11,14,15] On the basis of a number of seminal *in vivo* and *in vitro* studies, this enzyme has been proposed as a very promising target for the treatment of AD.[16,17] The inhibition of BACE1 can be used to titrate Aβ down to levels that will not support plaque formation.[18,19]

To achieve this goal a large number of X-ray structures (ca. 100) of the apo and inhibitor (transition state mimic hydroxyethylene-based peptidic (OM00-3 and OM99-2) and non-peptidic (SC6)) bound forms of BACE1 have been resolved.[20−24] These X-ray structures show that the N-terminal domain of BACE1 that is responsible for the catalytic activity exhibits 30% sequence identity to other members of this family such as pepsin, renin, and cathepsin D and possesses a common fold. The flap of this enzyme, which is the most relevant for drug designing, is formed by a N-terminal, 11 residue long fragment (Val67-Glu77) (Figure 1). The conserved Tyr71 residue of the flap form hydrogen bonds with the P1 and P2′ residues of APP (WT-substrate) and adopts different rotameric orientations to facilitate the movement of the flap (where P1, P2, ...

Received: January 18, 2011
Revised: April 7, 2011
Published: April 18, 2011

and P1′, P2′, ... consecutively denote the amino acid residues that flank the N and C-terminal of the substrate, respectively; Figure 2a).[24]

Another region of the enzyme known as the third strand (Lys107-Gly117) interacts with both the flap and active site through hydrogen bonds to stabilize the open or closed form of BACE1.[24] Several specific regions of the N-terminus [insert A (Gly158-Leu167)] and C-terminus [insert B (Lys218-Asn221), insert C (Ala251-Pro258), insert D (Trp270-Thr274), insert E (Glu290-Ser295), and insert F (Asp311-Asp317)] also facilitate the entry and binding of a substrate at the active site through their movements (Figure 1).[21] In addition, six N-terminal residues (Lys9-Tyr14) create a region known as the 10s loop that is located in the vicinity of insert A (Figure 1). In a previous molecular dynamics (MD) simulations study on the inhibitor (OM00-3) bound structure of BACE1, it was suggested that the flexible motions of the inserts D and F allow substrate entry and downward movements of inserts A and F make the active site flatter and wider and help with its binding.[25] These rearrangements are accompanied by structural alterations in the 10s loop and closing of the flap. A small number of conserved water molecules (W1 and W2) have also been reported to play critical roles in the catalytic functioning of BACE1.[26] Andreeva et al.[27] analyzed 82 cocrystal structures of aspartyl proteases and suggested specific roles of these water molecules. The W1 water molecule bridges the catalytic Asp dyad and is utilized in the hydrolytic cleavage of the peptide bond. However, the second water molecule (W2) participates in the H-bonding network to stabilize the flap in the closed conformation. Furthermore, it has been reported that a double mutation in the N-terminus region of APP (Lys670 → Asn and Met671 → Leu) known as the Swedish mutant (SW) accelerates the activity of BACE1 by 60-fold (Figure 2a).[28,29] The observed increase in the activity may be due to the differential substrates specificity of this enzyme,[30] i.e., the positioning of the substrate inside the active site and cleaving of the peptide bond. However, currently the mechanism of substrate specificity and interactions of the WT and SW substrates with the active site of the enzyme are not known.

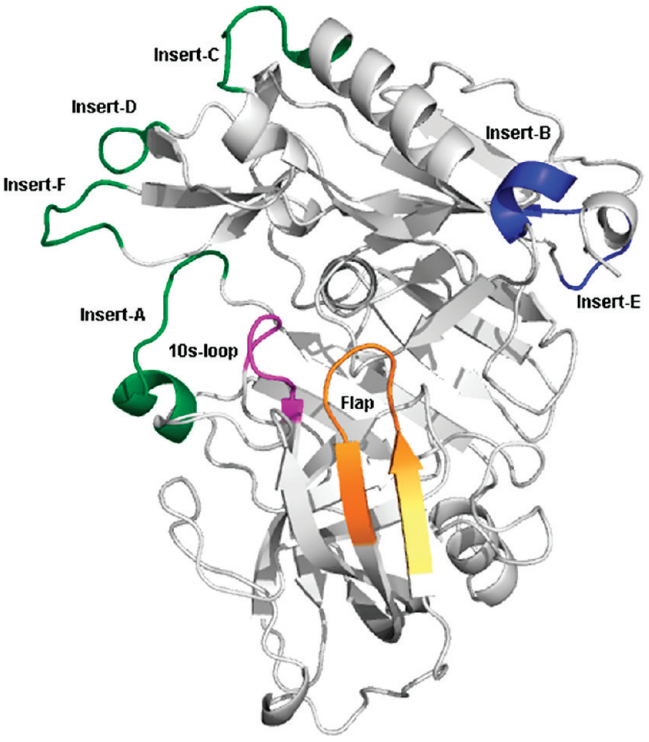

Figure 1. Key regions of BACE1 that participate in the substrate recognition from the X-ray structure (PDB ID: 1FKN); inserts A, C, D, and F (green), inserts B and E (blue), 10s loop (magenta), and flap (yellow).

Upon entering the active site, specific peptide bonds of the substrate are cleaved by the catalytically active dyad of BACE1. This dyad is formed by the Asp32 and Asp228 residues and both these residues interact with the conserved water molecule (W1) that is utilized for hydrolysis.[11,14,31] Recent X-ray and neutron diffraction data and theoretical calculations on the aspartyl proteases show that one of the Asp residues is protonated, and the second one is unprotonated.[32−35] BACE1 catalyzes the hydrolytic cleavage of the Met-Asp and Leu-Asp peptide bonds of the WT- and SW-substrate, respectively, through the following two overall reactions:

$$\text{Met-C(=O)-N(H)-Asp} + H_2O \rightarrow \text{Met-COOH} + \text{Asp-NH}_2 \quad (1)$$

$$\text{Leu-C(=O)-N(H)-Asp} + H_2O \rightarrow \text{Leu-COOH} + \text{Asp-NH}_2 \quad (2)$$

In the catalytic cycle, this enzyme utilizes the general acid/base

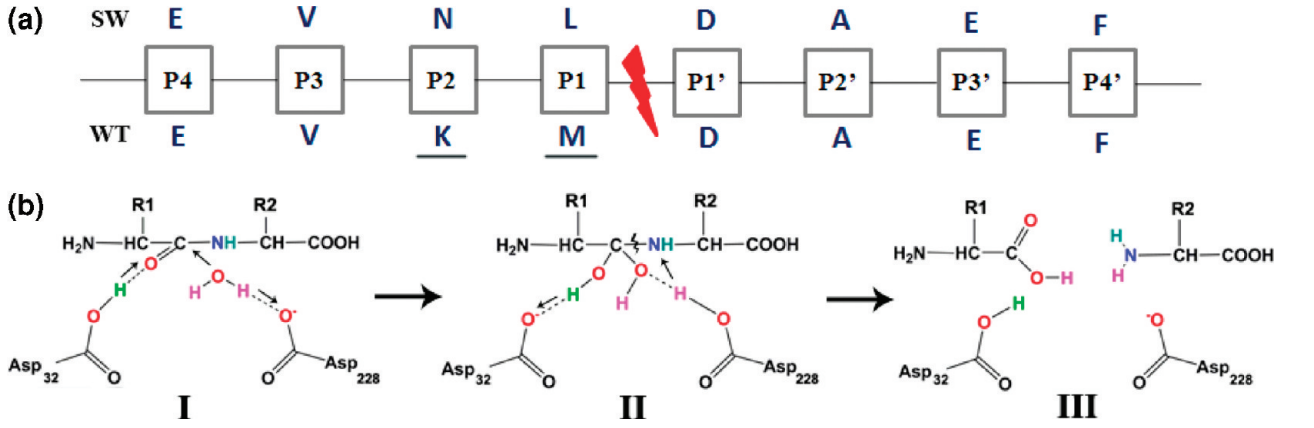

Figure 2. (a) Amino acid sequences of the wild type (WT) and Swedish (SW) substrates. The mutated residues are underlined, and the lightning sign marks the cleavage site. (b) General acid−base mechanism utilized by BACE1.[40,47]

dx.doi.org/10.1021/bi200081h |*Biochemistry* 2011, 50, 4337–4349

mechanism to cleave the peptide bond.[36] This mechanism (discussed below) has previously been theoretically studied for the other members of the aspartyl protease family such as HIV protease[37−41] and presenilin (PS1).[42] It has also been investigated by employing *ab initio* methods on simple models.[43−46] On the basis of available information, the peptide bond cleavage has been proposed to proceed through a two-step mechanism (Figure 2b).[40,47] In the first step, from the reactant (**I**) the unprotonated Asp228 functions as a base and abstracts a proton from the catalytic water to generate a hydroxyl ion (OH^-), which subsequently makes a nucleophilic attack on the carbonyl carbon atom of the peptide bond. In this process, Asp32 acts as an acid and concomitantly donates its proton to the carbonyl oxygen atom of the scissile peptide bond to generate the gem-diol intermediate (**II**). In **II**, two hydroxyl groups are coordinated to the carbon atom of the peptide bond. In the next step, the two aspartate residues switch their roles. Asp32 now functions as a base and abstract a proton from the hydroxyl group (−OH) of **II**. Here, Asp228, which became protonated in the previous step, plays the role of an acid and donates its proton to the amide nitrogen atom (−NH) of the scissile peptide bond. This process leads to the cleavage of the peptide bond to produce separated amine ($-NH_2$) and carboxyl (−COOH) terminals (**III**).[39,40] The experimentally measured k_{cat} = 2.45 s^{-1} for the SW-substrate is equivalent to a barrier of ca. 18.0 kcal/mol.[48] In a QM/MM study, Carloni et al. also showed that the formation of the gem-diol species for the Leu-Ala substrate peptide occurs through a barrier of ca. 20.0 kcal/mol.[38] However, currently the structural and mechanistic information on the hydrolytic cleavage of the Met-Asp and Leu-Asp peptide bonds of the WT and SW substrate, respectively, by BACE1 is not available.

In the present combined MD simulation and DFT study, the interactions of the WT-substrate with BACE1 and its cleavage mechanism have been investigated. In order to understand the increased activity of the SW variant with respect to the WT-substrate, the specific interactions of both the substrates (WT and SW) and energetics of their cleavage mechanisms are compared. To elucidate the specific changes introduced by the substrate binding, the structure of the substrate bound BACE1 (for both the WT and SW substrates) is also compared with its apo form. Furthermore, to validate the accuracy of the MD simulations, the structural features of the equilibrated SC6 inhibitor bound structure are compared with the corresponding X-ray structure (PDB ID: 2QMG). The structures obtained from the MD simulations (BACE1-WT and BACE1-SW) were subsequently utilized to investigate the mechanisms for the cleavage of the Met-Asp and Leu-Asp peptide bonds of the WT- and SW-substrate, respectively. These calculations will provide structural and mechanistic information concerning the catalytic functioning of this critical enzyme. This information might also be helpful to understand the activities of other members of this family. The great deal of available experimental and theoretical data has provided an ideal platform to perform this study.

COMPUTATIONAL PROCEDURE

Computational Modeling. The models for the WT- and SW-substrate were constructed from the OM99-2 inhibitor bound X-ray structure of BACE1 in the flap closed conformation (PDB ID: 1FKN).[21] The OM99-2 inhibitor is a transition state mimic of the SW-substrate designed by incorporating a statin group ($-CH_2-CH(OH)-$) between the P1 (Leu) and P1′ (Asp) amino acid residues and substituting P1′ residue by Ala. The starting structure for the SC6 inhibitor was taken from its cocrystal structure (PDB ID: 2QMG) in the closed form.[49] The non-peptidic (SC6) and peptidic (OM99-2) inhibitors were then placed in the active site of the X-ray structure (PDB ID: 1W50) of apo form of this enzyme, in the flap open conformation, by superposing the structures.[22] The missing insert A (158-167) in the apo structure (PDB ID: 1W50) was incorporated from another X-ray structure (PDB ID: 1FKN). The structure of insert A in this structure was energy minimized by keeping the rest of the enzyme fixed from the X-ray structure (PDB ID: 1W50). Since the structure of the OM99-2 inhibitor is similar to the SW-substrate, it was converted to this substrate by substituting the statin group with the actual peptide bond and Ala at the P1′ position with the Asp residue. The WT-substrate was then generated from the SW-substrate by mutating Leu (P1) and Asn (P2) with the Met and Lys residues, respectively (Figure 2a). These substitutions were made by using the Swiss PDB viewer program (SPDBV), and the energetically favorable rotamers of the aforementioned amino acids were chosen to minimize the bad contacts with BACE1. On the basis of the available experimental and theoretical information, Asp32 and Asp228 were kept in the protonated and unprotonated form, respectively.[32−35] All these structures were subsequently equilibrated in a multistep procedure. In the first step, only the structures of the substrates and inhibitor in each case were minimized by keeping the coordinates of the apo-enzyme constraints from the X-ray structure (PDB ID: 1W50). In the second step, all the constraints were removed and the structures of the enzyme−substrate complexes were energy minimized with a steepest descent method for 3000 steps. The results of these minimizations produced the initial structures for the position restrained MD simulations. In the next step, these structures were subjected to 300 ps MD simulations in which the protein was kept fixed to allow water molecules to enter inside the protein and adjust their positions around it. These structures were subsequently used as starting points for the 20 ns BACE1-SW, BACE1-WT, and BACE1-SC6 all-atom MD simulations in aqueous solution. In the apo-BACE1 simulations, the coordinates were taken from its X-ray structure (PDB ID: 1W50) including the insert A region from the X-ray structure (PDB ID: 1FKN).

Molecular Dynamics Simulations. All molecular dynamics (MD) simulations were performed using the GROMACS software package[50,51] utilizing the OPLS-AA[52,53] force field. The topology of the SC6 inhibitor was built using the MKTOP Perl script developed at the Federal University of Rio degenerio, Brazil.[54] The partial atomic charges for this compound were obtained by fitting ESP charge using the ChelpG[55,56] method at B3LYP/6-31G(d)[56,57] level using the Gaussian09 program.[58] In the simulations, the structures were placed in the center of a box with dimensions 8.0 × 8.0 × 8.0 nm. The box contained over (∼15 000) of TIP4P[59] water molecules, i.e., ca. 66 000 atoms in total. Some water molecules were replaced by sodium ions to neutralize the systems. The MD simulations were carried out with a constant number of particles (N), pressure (P), and temperature (T), i.e., *NPT* ensemble. The SETTLE algorithm was used to constrain the bond length and angle of the water molecules,[60] while the LINCS algorithm is used to constrain the bond length of the peptides.[61] The long-range electrostatic interactions were calculated by the particle-mesh Ewald (PME) method.[62,63] A constant pressure of 1 bar was applied with a coupling constant of 1.0 ps; protein, water molecules, and ions were coupled separately to a bath at 300 K with

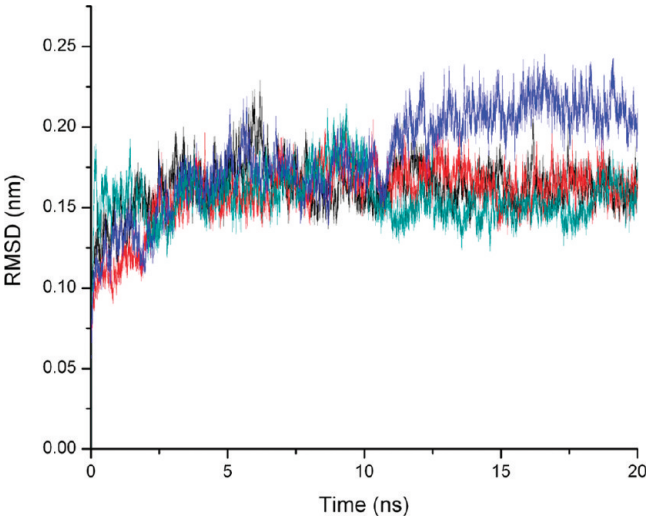

Figure 3. Rmsd of the BACE1-WT (black), BACE1-SW (cyan), BACE1-SC6 (red), and apo-BACE1 (blue) trajectories plotted against time.

a coupling constant of 0.1 ps. The PBC (periodic boundary condition) was applied, and the equation of motion was integrated at time steps of 2 fs. The tools available in GROMACS program package and the YASARA program[64] have been utilized to analyze the different MD trajectories. The PyMol[65] and VMD[66] software were also extensively used for visualizations and the preparation of structural diagrams presented in this study. The relative electrostatic binding energies[67] for the enzyme−substrate complexation were computed by solving linearized Poisson−Boltzmann equation utilizing APBS (Adaptive Poisson−Boltzmann Solver) software.[68,69] The details of these computations are provided in the Supporting Information. The accuracy of the GROMACS program was also tested by performing BACE1, BACE1-SC6 (cocrystal structure (PDB ID: 2QMG)), and BACE1-SC6 (SC6 bound to the apo-form of the enzyme) simulations utilizing the Desmond program[70] using the OPLS-AA[52,53] force field. The analysis of these trajectories indicates that both programs (GROMACS and Desmond) provided very similar results (Figure S1 in the Supporting Information).

Modeling for DFT Calculations. The most representative structures derived from the 20 ns BACE1-WT and BACE1-SW MD simulations were used to create starting models for the DFT calculations. Both substrates were modeled using the tetrapeptide sequences, i.e., Lys-Met-Asp-Ala for the WT-substrate and Asn-Leu-Asp-Ala for the SW-substrate. In the active site models of BACE1, the catalytically active Asp32 and Asp228 residues, two conserved water molecules (W1 and W2), and four surrounding residues (Arg235, Thr231, Ser35, and Tyr71) were included. These models contain in total 137 atoms for the WT-substrate and 132 atoms for the SW-substrate and represent the common structural features of the actives sites of BACE1. In order to retain the strain exerted by the surrounding protein on the active site, the positions of some of the amino acid residues (shown with asterisk sign in the corresponding figures) are constrained from the structures equilibrated using MD simulations. Asp32 and Asp228 residues were modeled as acetic acid, Thr231 as $CH_3-CH(OH)-CH_3$, Ser35 as CH_3-CH_2-OH, Tyr71 as $CH_3CH_2C_6H_5OH$, and Arg235 as $CH_3-NH-C(=NH_2)^+(-NH_2)$. This kind of modeling has been widely used in quantum chemical studies.[71−73] The overall charge state of the system is 0 for the WT-substrate and −1 for the SW-substrate, and they exist in the singlet ground states.

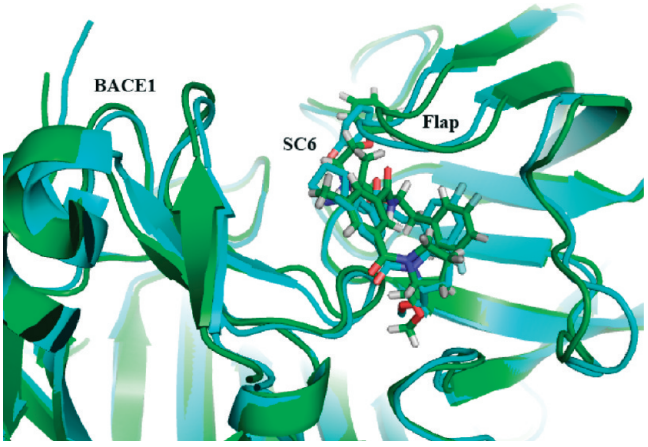

Figure 4. Superposition of the most representative structure derived from the BACE1−SC6 simulation (green) with the corresponding X-ray structure (cyan) (PDB ID: 2QMG).

Quantum Mechanical Calculations. All calculations were performed using the Gaussian 09 program.[58] The geometries of reactants, intermediates, transition states, and products were optimized without any symmetry constraints using the B3LYP method and 6-31G(d) basis set.[56,57,74] The accuracy of the B3LYP method used in this study to calculate the reaction barrier is between 3 to 5 kcal/mol.[40,72] All degrees of freedom were optimized and the transition states obtained were confirmed to have one imaginary frequency corresponding to the reaction coordinate. The final energetics of the optimized structures was improved by performing single-point calculations using the triple-ζ quality basis set 6-311+G(d,p). Since it was computationally unfeasible to calculate unscaled zero-point energy and thermal corrections using the triple-ζ quality basis set, these effects were estimated at the B3LYP/6-31G(d) level and added to the final B3LYP/6-311+G(d,p) energetics. This type of correction is an adequate approximation and has commonly been used in quantum chemical studies.[72,75] The dielectric effects from the surrounding environment were estimated using the dielectric constant (ε) of 4.33, corresponding to diethyl ether, utilizing the self-consistent reaction field IEF-PCM method[76] at the B3LYP/6-31G(d) level. In general, when models with the same charge are used, the relative dielectric effects are not very sensitive to the methods used or to the value chosen for the dielectric constant. Throughout the paper the energies obtained at the B3LYP/(6-311+G(d,p)) + zero-point energy (unscaled) and thermal corrections (at 298.15 K and 1 atm) + solvent effects are discussed, while the energies without solvent effects are provided in parentheses.

RESULTS AND DISCUSSION

In the present study, interactions of the WT- and SW-substrate with the specific regions of BACE1 and their cleavage mechanisms have been elucidated. In particular, four independent all-atom 20 ns MD simulations (BACE1-WT, BACE1-SW, BACE1-SC6, and apo-BACE1) have been performed in aqueous solution. The root-mean-square deviations (rmsd) of the MD trajectories indicate that the structures in all four trajectories are well equilibrated (BACE1-SC6, BACE1-WT, and BACE1-SW

simulations only after 5 ns and apo-BACE1 after 10 ns) (Figure 3). The structures derived from these simulations were subsequently used to investigate mechanisms for the cleavage of the Met-Asp and Leu-Asp peptide bonds of the WT and SW substrates, respectively.

The MD simulations are validated by comparing the structural features of the most representative structure derived from the BACE1-SC6 simulation with the corresponding X-ray structure (PDB ID: 2QMG). Both these structures superpose well to each other, and the overall rmsd between these two structures is only 1.7 Å (Figure 4). The rmsd for the critical flap region (67−77) and the 10s loop (9−14) are also found to be quite small, i.e., 1.3 and 1.0 Å, respectively. Furthermore, the computed *B*-factors of the C^{α} atoms calculated from the root-mean-square fluctuation (rmsf), using the $B = (8\pi^2/3) \times (\text{rmsf})^2$ expression, are in good agreement with the crystallographic factors of the X-ray structure (PDB ID: 2QMG) (Figure 5). The opening and closing of the flap (Val67-Glu77) region is critical for both the substrate binding and catalytic activity of BACE1.[16,24] The movement of the flap upon the substrate binding is monitored by the changes in the three interatomic distances (C^{α}(Thr72)−C^{β}(Asp32), C^{α}(Thr72)−C^{α}(Thr329), and OG1(Thr72)−NH1(Arg235)).[26] The C^{α}(Thr72)−C^{β}(Asp32) distance defines the motion of the flap and considered to be the key parameter in the substrate recognition.[26] The Thr72 residue is located at the tip of the flap, and Asp32 constitutes the catalytic dyad that plays an important role in the hydrolysis of the substrate. The C^{α}(Thr72)−C^{α}(Thr329) distance provides a measure of the gap between the tip of the flap region and C-terminal of BACE1. The OG1(Thr72)−NH1(Arg235) distance is important because both Thr72 and Arg235 residues of BACE1 have been observed to interact with the inhibitor and suggested to be involved in the ligand−BACE1 interactions.[21,49]

The time evolution of the C^{α}(Thr72)−C^{β}(Asp32) distance indicates that the flap of the BACE1−SC6 complex closes around 3 ns (Figure 6). This distance decreases from 16.7 Å (apo crystallographic distance) to 12.4 Å and remains that way for the rest of the simulation. It is in excellent agreement with the distance of 12.0 Å observed in the crystal structure of the BACE1-SC6 complex (PDB ID: 2QMG).[49] The remaining two distances C^{α}(Thr72)−C^{α}(Thr329) and OG1(Thr72)−NH(Arg235) are also found to be in good accord and only slightly longer by 1.0 and 0.3 Å, respectively, than the corresponding distances in the X-ray structure (PDB ID: 2QMG). The computed interaction energy per residue for the residues within 5 Å of SC6 is also very similar in the equilibrated and X-ray structures (Figure S2 in the Supporting Information). Furthermore, the BACE1-SC6 simulation accurately reproduced the position of the W2 water molecule and its interactions with the Ser35, Asn37, and Tyr71 residues from the X-ray structure (Figure S3 in Supporting Information). These hydrogen-bonding interactions have also been observed in the previous MD simulations studies.[25,26] These results explicitly indicate that the MD simulation accurately described the process of flap closing upon the binding of the SC6 inhibitor in the open flap conformation of the enzyme.

Interactions of the WT-Substrate with BACE1. The flap region in the apo form of BACE1 is very flexible and frequently interchanges between the open and close conformations (Figure 6).[26] However, upon ligand binding (substrate or inhibitor) the flap region adopts the close conformation, but the extent of closing might depend on the nature of the ligand. Here, the process of flap closing for the binding of the WT-substrate is compared with the binding of the SC6 inhibitor. The plot of the C^{α}(Thr72)−C^{β}(Asp32) derived from the BACE1-WT trajectory

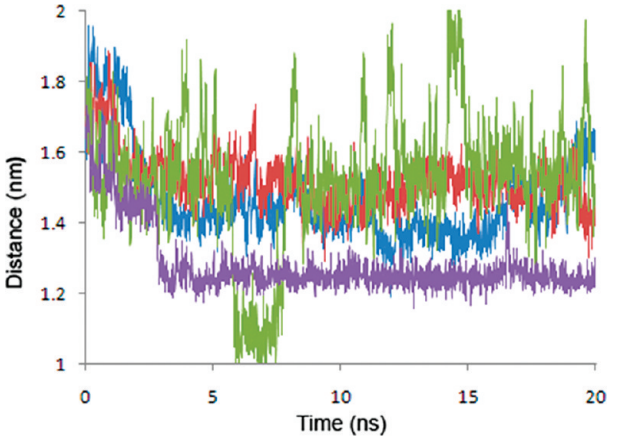

Figure 6. Time evolution of the C^{α}(Thr72)−C^{β}(Asp32) distance for the BACE1-WT (red), BACE1-SW (blue), BACE1-SC6 (violet), and apo-BACE1 (green) trajectories.

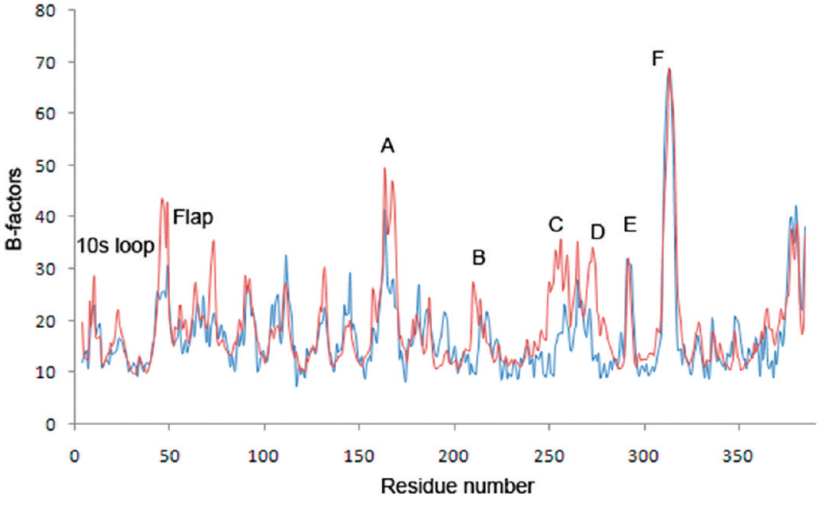

Figure 5. Comparison between the measured (blue) and computed (red) *B*-factors.

dx.doi.org/10.1021/bi200081h |*Biochemistry* 2011, 50, 4337–4349

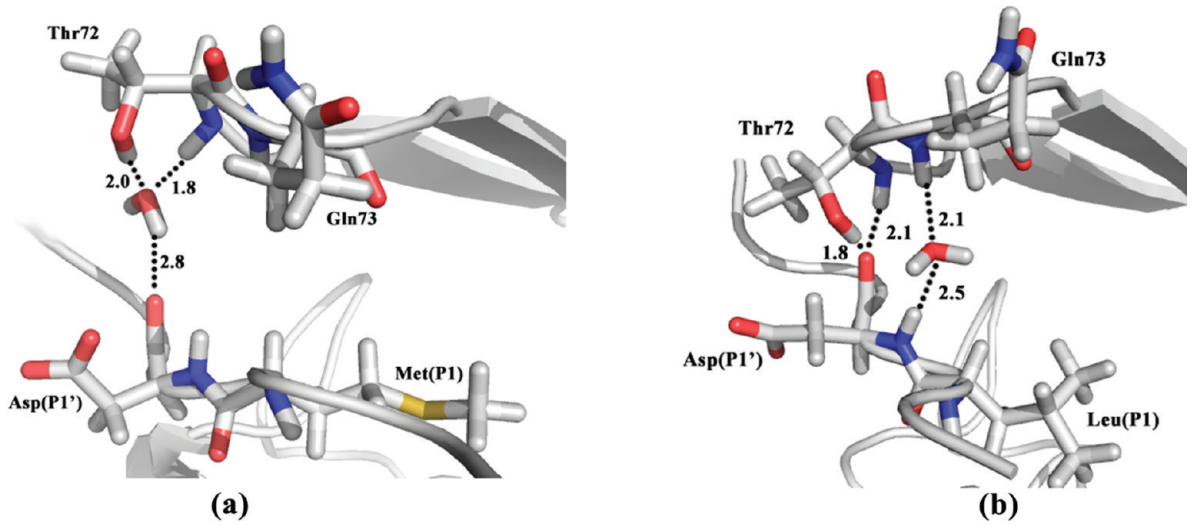

Figure 7. Water-mediated interaction of Thr72 located at the tip of the flap with the substrate: (a) WT-substrate and (b) SW-substrate.

Table 1. C^{α}(Thr72)−C^{β}(Asp32), C^{α}(Thr72)−C^{α}(Thr329), and OG1(Thr72)−NH1(Arg235) Distances (in Å) Computed from the Most Representative Structures Obtained from the MD Simulations

distance	WT	SW	SC6 (MD)	SC6 (X-ray)
C^{α}(Thr72)−C^{β}(Asp32)	14.9	14.2	12.4	11.9
C^{α}(Thr72)−C^{α}(Thr329)	11.2	10.8	9.9	8.9
OG1(Thr72)−NH1(Arg235)	6.4	6.0	5.2	4.9

indicates the closing of the flap around 3 ns (Figure 6). This time frame is also similar to the one observed for the binding of the SC6 inhibitor in the BACE1-SC6 simulation. The Thr72 residue located at the tip of the flap interacts with Asp(P1′) of the substrate through a bridging water molecule. Both the side chain and backbone of Thr72 form strong hydrogen bonds with the water molecule that in turn forms a single hydrogen bond with the backbone carbonyl (C═O) group of Asp(P1′) (Figure 7a). The presence of the Tyr71(O)-Trp76(N) hydrogen bond in the most representative structures derived from the BACE1-WT and BACE1-SC6 trajectories indicates the closing of the flap in both the cases. However, the average C^{α}(Thr72)−C^{β}(Asp32) distance of 14.9 Å (Table 1) computed from the BACE1-WT simulation is ca. 2.5 Å longer than the one obtained from the BACE1-SC6 simulation. This difference shows that in comparison to the SC6 inhibitor the flap is more open in the presence of the WT-substrate at the active site. In the WT-substrate bound structure, the C^{α}(Thr72)−C^{α}(Thr329) distance of 11.2 Å is also 1.3 Å longer than the BACE1-SC6 case, which indicates that the enzyme remains more open upon the binding of former. In the equilibrated structure, similar to other two distances, the distance between the side chains of Thr72 and Arg235 (OG1(Thr72)-NH1(Arg235)) of 6.4 Å, is longer (by 1.2 Å) than the one obtained from the BACE1-SC6 simulation (Table 1). The computed differences in these distances between the BACE1-WT and BACE1-SC6 simulations clearly indicate that the active site is relatively more open upon the binding of the WT substrate. This inference is also supported by the volume of the active site computed using a single water molecule with van der Waals sphere of radius of 1.6 Å using the SiteMap module of Schrodinger suit of program.[77] Throughout the simulation, volume of the active site for the WT-substrate is observed to be greater than the SC6 inhibitor, i.e., 520 $Å^3$ computed for the former is 380 $Å^3$ more than for the latter (Figure 8). These results explicitly show that, in comparison to SC6, the flap of BACE1 is more open, and as a result the active site is more expanded in the presence of the WT-substrate.

Hydrophobic interactions also play an important role in positioning of the WT-substrate inside the active site.[78] In the equilibrated structure, the Met (P1) residue of the WT substrate makes hydrophobic contacts with Tyr71 and Phe108 residues of BACE1 through CH_3-π type of interactions. Val (P3) forms hydrophobic contact with Trp115 of the enzyme. The WT-substrate was also found to form a small number of hydrogen bonds (4−5) with BACE1 (Figure 9). The Glu (P4), Met (P1), Asp (P1′), and Ala (P2′) residues of the substrate are involved in forming the specific hydrogen bonds with the enzyme (Table 2). For instance, Glu (P4) interacts with the side chain of Asn233 and also makes a strong hydrogen bond with the Lys (P2) residue (Figure 10a). These hydrogen-bonding interactions are quite important and the substitution of Glu with Gln or Asp has been experimentally observed to decrease the catalytic efficiency of BACE1.[79] The positively charged Lys (P2) residue of the WT-substrate does not interact with the positively charged Arg235 and instead moves away to form a hydrogen bond with the negatively charged Glu (P4) of the substrate. The electrostatic binding energy computed using APBS (Adaptive Poisson−Boltzmann Solver) is −4.6 kcal/mol.

The binding of the WT-substrate in the apo form of the enzyme introduces substantial changes in the key regions (inserts A, D, and F) and 10s loop of BACE1 (Figure S4 in the Supporting Information). The α-helical conformation of insert A observed in the apo-form is lost upon binding of the WT-substrate. In contrast, the binding of SC6 retains the α-helical conformation of insert A from the X-ray structure. Rather interestingly, the binding of this substrate does not alter the positions of insert D and 10s loop that are located just above insert A. However, the location of insert F is significantly different in the substrate bound form. Because of the formation of hydrogen bonds between Glu310 (insert F) with the Lys9 and Gln12 (10s loop) in the apo-form of the enzyme, the Val309-Val312 region of the insert F

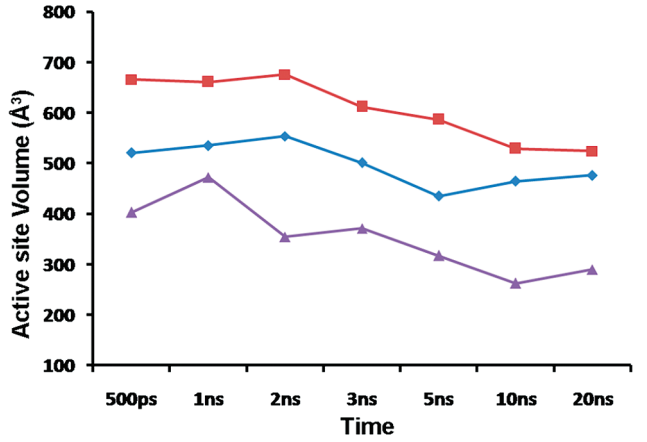

Figure 8. Variation in the volume of the active site with time from the BACE1-WT (red), BACE1-SW (blue), and BACE1-SC6 (violet) trajectories.

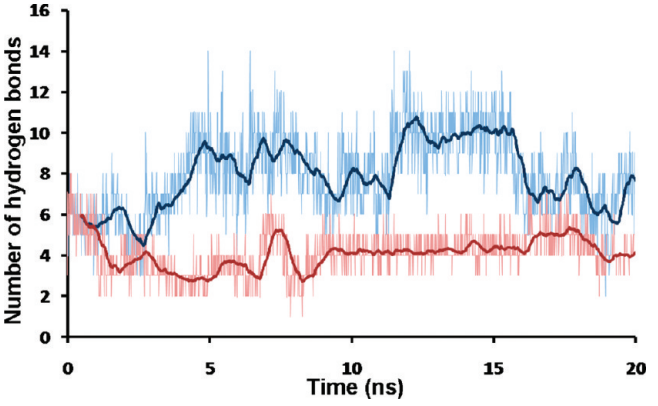

Figure 9. Time evolution of the number of H-bonds between BACE1 and the substrate from the BACE1-WT (red) and BACE1-SW (blue) trajectories.

shifts toward the 10s loop and insert A. However, in the WT-substrate bound BACE1 only one of these two hydrogen bonds, Gly310(insert F)-Lys9(10s loop), remains intact to facilitate the movement of insert F away from the insert A and 10s loop. In the case of SC6 inhibitor also insert F displays the similar movement. These results show that there are substantial differences between the interactions of the WT-substrate and SC6 with BACE1 that influence the structures of the several key regions of the enzyme.

Interactions of the SW-Substrate with BACE1. The variation in the C^{α}(Thr72)−C^{β}(Asp32) distance shows that, similar to the WT-substrate, the flap closes around 3 ns in the presence of the SW-substrate (Figure 6). In the most representative structure derived from the BACE1-SW trajectory, the average C^{α}-(Thr72)−C^{β}(Asp32) distance of 14.2 Å is found to be 0.7 Å shorter than the WT-substrate bound structure (Table 2). This suggests that the flap is slightly more closed due to the binding of the SW-substrate. The variation in the extent of the flap closing for both the substrates might also be caused by the substantial differences observed in their interactions with the flap. The backbone carbonyl (C═O) group of Asp(P1′) of the SW-substrate forms two strong hydrogen bonds with the side chain and backbone of Thr72 located at the tip of the flap. In addition, the amine (−NH) part of the backbone amide (−CONH) group

Table 2. Hydrogen-Bonding Distances (Considering Only the Distances between Heavy Atoms) between BACE1 and the Substrate (WT and SW)

	residue (substrate)	atom	residue (BACE1)	atom	Å
WT					
P4	Glu	OE2	Asn233	ND2	2.6
P1	Met	O	Asp32	OD2	3.2
P1′	Asp	OD1	Lys224	NZ	2.6
		OD2	Arg235	NH1	2.8
P2′	Ala	N	Tyr198	OH	2.3
SW					
P4	Glu	OE2	Asn233	ND2	2.9
			Lys321	NZ	2.5
		OE1	Arg307	NH2	2.6
P3	Val	O	Thr232	N	2.8
P2	Asn	ND2	Arg235	NE	2.8
P1	Leu	O	Asp32	OD2	3.0
P1′	Asp	O	Thr72	OG1	2.6
		OD1	Arg235	NH1	2.7
		O	Thr72	N	2.8
P3′	Glu	OE1	Lys224	NZ	2.8

of Asp(P1′) indirectly interacts with the backbone of Gln73 through a bridging water molecule (Figure 7b). On the other hand, for the WT-substrate only the backbone carbonyl (C═O) group of Asp(P1′) associates with Thr72 by forming a hydrogen bond with a water molecule that strongly interacts with both the side chain and backbone of Thr72. The C^{α}(Thr72)−C^{α}(Thr329) distance for the SW-substrate is also 0.4 Å shorter than for the WT-substrate, i.e., 10.8 and 11.2 Å for the former and latter, respectively. This difference also indicates that the flap is a little more closed for the SW-substrate. In addition, the third critical distance (OG1(Thr72)−NH1(Arg235) = 6.0 Å) for the SW-substrate was computed to be 0.4 Å shorter than its WT counterpart (Table 1). Furthermore, the overall volume of the active site throughout the trajectory and in the most representative structure (470 $Å^3$) is substantially smaller than the WT substrate (Figure 8). All these structural parameters indicate that, in comparison to the WT-substrate, the flap is more closed and the active site is more constricted upon binding of the SW substrate.

This substrate (SW) also interacts with the active site through specific hydrophobic and hydrogen-bonding interactions. Similar to the Met(P1) residue of the WT-substrate, the Leu(P1) of this substrate associates through hydrophobic contacts and CH_3−π interactions with Tyr71 and Phe108, respectively. However, here the interaction of Val(P3) of the substrate with Trp115, as observed for the WT-substrate, is disrupted, and the substrate reorients and positions itself within van der Waals (vdw) radius of Ile110. The SW-substrate forms around two times (8−10) more hydrogen bonds with BACE1 than the WT-substrate (Figure 9). The Glu (P4), Val (P3), Asn (P2), Leu (P1), Asp (P1′), and Glu (P3′) residues of the SW-substrate are involved in forming these hydrogen bonds (Table 2). Glu(P4) interacts with the side chains of Asn233, Lys321, and Arg307 through three hydrogen bonds, i.e., the OE2 atom of the Glu residue forms hydrogen bonds with Asn233 and Lys321 and the OE1 atom with Arg307 (Figure 10b). Among these hydrogen bonds, the Glu(P4)-Arg307 bond has been reported to influence the catalytic activity of the enzyme.[79] The loss of this interaction

dx.doi.org/10.1021/bi200081h |*Biochemistry* 2011, 50, 4337–4349

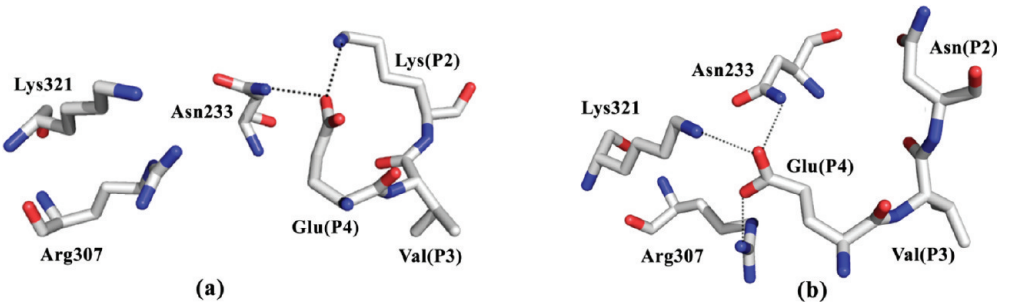

Figure 10. (a) Interaction of Glu(P4) with Asn233 and Lys(P2) in the BACE1-WT complex. (b) Interaction of Glu(P4) with Asn233, Arg307, and Lys321 in the BACE1-SW complex. (Hydrogen atoms are removed for clarity.)

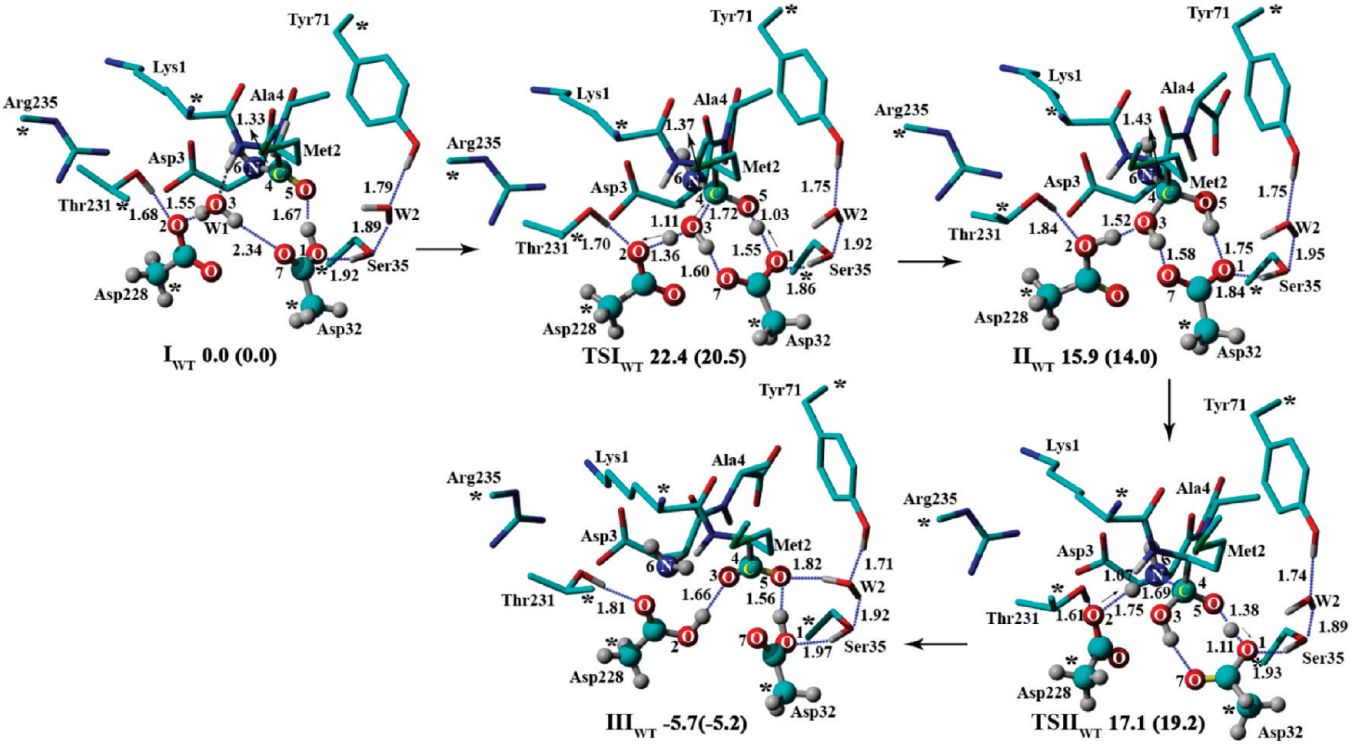

Figure 11. Structures (in Å) and energies (in kcal/mol) of the reactant, intermediate, transition states (optimized), and the product for the cleavage of the Met2-Asp3 peptide bond of the WT-substrate. The noncritical hydrogen atoms have been omitted in the figure, and the frozen atoms are shown with the asterisk mark.

could be responsible for its reduced enzymatic activity for the WT-substrate. The backbones of Val(P3) and Thr232 also form a hydrogen bond with each other, and the backbones of Leu(P1) and Asp(P1′) interact with the side chains of Asp32 and Thr72, respectively. The Arg235 residue at the active site of BACE1 has been reported to play a critical role in the substrate recognition.[30] Unlike the Lys(P2) residue of the WT substrate, Asn(P2) of the SW-substrate forms a hydrogen bond with this residue. For the SW-substrate, the electrostatic binding energy of −6.5 kcal/mol computed using APBS is 1.9 kcal/mol lower than the corresponding energy for the WT-substrate. On the basis of these results, it can be concluded that, in comparison to the WT-substrate, BACE1 exhibits higher affinity for the SW-substrate.

In the presence of the SW-substrate, inserts A, D, and F and the 10s loop of the enzyme adopt significantly different conformations than in the case of the WT-substrate. Insert A loses its overall α-helical conformation upon the binding of both the substrates, but its Asn162-Glu165 segment shifts toward the active site for the SW-substrate. This shift may be caused by the motion of the 10s loop in this direction that further pushes the fragment. However, for the WT-substrate this loop is positioned away from the active site at exactly the same location as predicted for the apo-form of the enzyme. No noticeable change was observed in the structure and location of the insert D upon binding of both the substrates. In the BACE1-SW structure, the Val309-Val312 fragment of Insert F is more open and shifted away from the active site than in the BACE1-WT complex. However, similar to the BACE1-WT complex, the inserts A and F interact with each other through the Glu310 (insert F)-Lys9 (10s loop) hydrogen bond.

Catalytic Mechanism of BACE1. In this section, the most representative structures derived from the BACE1-WT and BACE1-SW simulations were utilized to develop initial pruned

dx.doi.org/10.1021/bi200081h |*Biochemistry* 2011, 50, 4337–4349

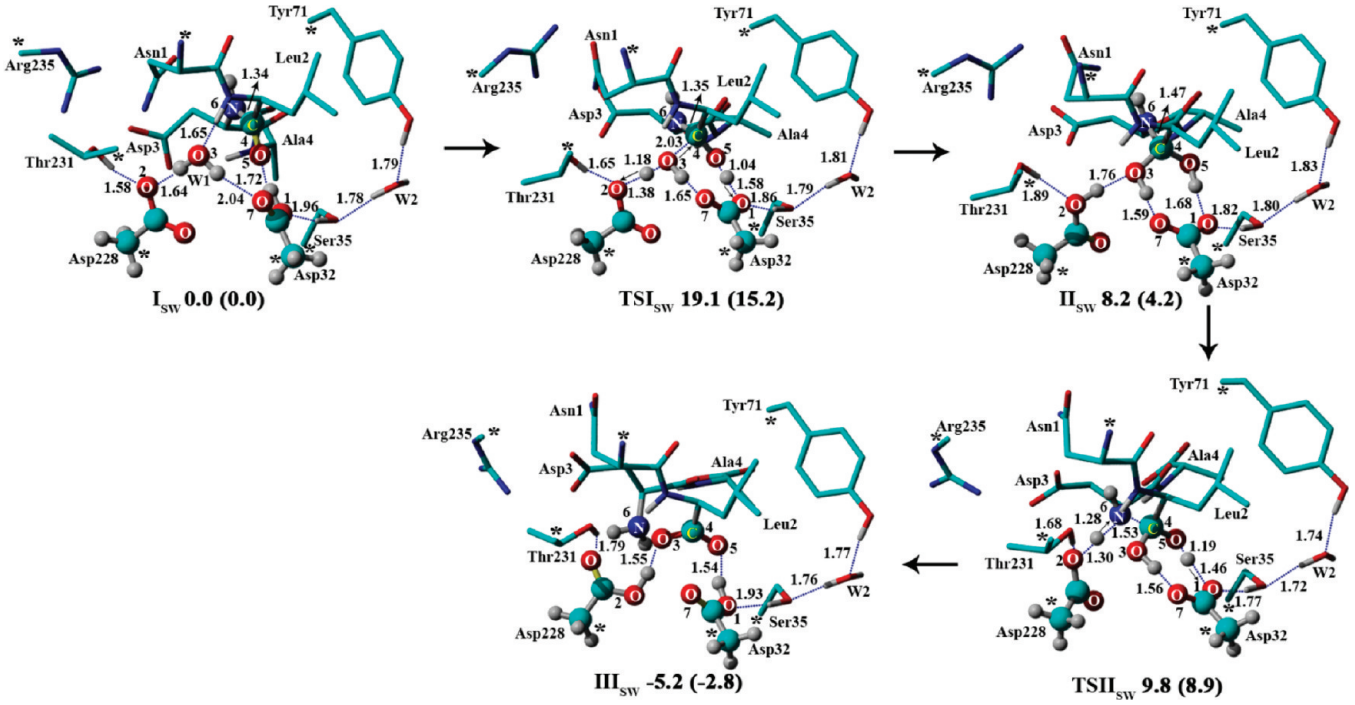

Figure 12. Structures (in Å) and energies (in kcal/mol) of the reactant, intermediate, transition states (optimized), and the product for the cleavage of the Leu2-Asp3 peptide bond of the SW-substrate. The noncritical hydrogen atoms have been omitted in the figure, and the frozen atoms are shown with the asterisk mark.

models of the enzyme−substrate complexes. In the absence of the substrate bound X-ray structures, they provide good starting structures. It is noteworthy that these models were used only as the starting structures and subjected to further optimizations at the B3LYP/6-31G(d) level of theory to investigate mechanisms for the hydrolytic cleavage of the Met2-Asp3 and Leu2-Asp3 peptide bond of the WT- and SW-substrate, respectively, by BACE1. This approach to explore the potential energy surface (PES) has previously been successfully applied to study mechanisms of a large number of enzyme-catalyzed reactions.[42,71,73,75,80−84]

Reactions 1 and 2 are computed to be endothermic by 4.0 and 8.8 kcal/mol, respectively. BACE1 utilizes the general acid−base mechanism to catalyze these reactions. This mechanism proceeds through the following two steps: (1) generation of the gem-diol intermediate and (2) cleavage of the peptide bond.

Formation of the Gem-Diol Intermediate. During the optimization, the starting models of the reactants derived from the MD simulations undergo only minor changes and largely retain their initial structures. In the optimized reactant for the WT substrate ($\mathbf{I_{WT}}$), the active site water molecule (W1, H_2O^3) interacts with the catalytic diad formed by Asp32 (protonated) and Asp228 (unprotonated) through hydrogen bonds (O^3H-O^7= 2.34 Å and O^3H-O^2 = 1.55 Å) (Figure 11). The reactant for the SW-substrate ($\mathbf{I_{SW}}$) forms the similar complex, but the O^3H-O^7 bond distance in $\mathbf{I_{SW}}$ is 0.30 Å shorter than the corresponding bond in $\mathbf{I_{WT}}$(O^3H-O^7 = 2.04 Å and O^3H-O^2 = 1.64 Å) (Figure 12). However, in both $\mathbf{I_{WT}}$ and $\mathbf{I_{SW}}$, the N−H backbone of Met2 and Leu2, respectively, makes a hydrogen bond with the O^3 atom of the W1 molecule. In addition, the side chain (O^1-H) of Asp32 makes hydrogen bond with the carbonyl oxygen of the Met2 (O^1-H-O^5 = 1.67 Å) and Leu2 residues (O^1-H-O^5 = 1.72 Å) of the WT- and SW-substrate, respectively. In both reactants ($\mathbf{I_{WT}}$ and $\mathbf{I_{SW}}$), the Asp32 and Asp228 residues interact with the neighboring Ser35 and Thr231, respectively, through hydrogen bonds.

In the first step of the mechanism, Asp32 functions as an acid, while Asp228 as a base. Here, from $\mathbf{I_{WT}}$ and $\mathbf{I_{SW}}$, the unprotonated Asp228 abstracts a proton from the active site water molecule (H_2O^3) to create the hydroxyl ion (O^3H^-). The $-O^3H$ ion concomitantly makes a nucleophilic attack to the carbonyl carbon atom (C^4) of the Met2-Asp3 and Leu2-Asp3 scissile bonds of the WT and SW substrates, respectively. In this process, Asp32 acts as an acid and simultaneously transfers a proton to the carbonyl ($C^4=O^5$) group of the scissile peptide bond. In comparison to $\mathbf{I_{WT}}$, the O^3 and C^4 atoms of $\mathbf{I_{SW}}$ possess extra charge (0.06 and 0.14 e, respectively), which makes W1 and carbonyl carbon (C^4) atom of $\mathbf{I_{SW}}$ a superior nucleophile and electrophile, respectively. This suggests that, in comparison to the WT-substrate, the SW-substrate is more susceptible for this reaction. In the optimized transition state ($\mathbf{TSI_{WT}}$) for the WT-substrate, all the relevant bond distances indicate that this process is concerted (O^2-H = 1.36 Å, O^3-H = 1.11 Å, O^3-C^4 = 1.72 Å, O^1-H = 1.55 Å, and O^5-H = 1.03 Å). In particular, the O^3-H bond distance in $\mathbf{TSI_{SW}}$ is 0.07 Å longer than in $\mathbf{TSI_{WT}}$, which shows that the water molecule is more activated in the former. The barrier of 22.4 kcal/mol for this process for the WT-substrate is 3.3 kcal/mol higher than the one computed for the SW-substrate (19.1 kcal/mol from $\mathbf{I_{SW}}$). This is the rate-limiting step of the entire mechanism for both the substrates. Considering the accuracy (3−5 kcal/mol) of the B3LYP functional in computing barriers, the calculated barrier for this step in this study is in agreement with the experimentally measured barrier of ca. 18.00 kcal/mol for the WT-substrate.[48] However, the accuracy of the computed barrier should be validated using QM/MM approaches. Furthermore, it is quite similar to the barrier of ca. 20 kcal/mol calculated for the cleavage of the Leu-Ala peptide bond in a previous QM/MM study.[38]

dx.doi.org/10.1021/bi200081h |*Biochemistry* 2011, 50, 4337–4349

In order to study the influence of the structures of the reactants ($\mathbf{I}_{WT}$ and $\mathbf{I}_{SW}$) on the computed difference of 3.3 kcal/mol between the barriers, this step was also investigated using a different set of snapshots taken at the 10th ns of the BACE1-WT and BACE1-SW simulations. This approach has previously been applied to study mechanisms of acetylcholinesterase[85] and triosephosphate isomerase.[86] The optimized structures of the pruned models of reactants ($\mathbf{I'}_{WT}$ and $\mathbf{I'}_{SW}$ for the WT- and SW-substrate, respectively) using these trajectories are significantly different from $\mathbf{I}_{WT}$ and $\mathbf{I}_{SW}$ (Figures S5 and S6 in Supporting Information). From $\mathbf{I'}_{WT}$ and $\mathbf{I'}_{SW}$, the difference in barrier (4.6 kcal/mol) was found to be only 1.3 kcal/mol higher than the one calculated using $\mathbf{I}_{WT}$ and $\mathbf{I}_{SW}$ (3.3 kcal/mol).

The activation of H_2O^3 (W1) in this step leads to the creation of the gem-diol intermediate ($\mathbf{II}_{WT}$ and $\mathbf{II}_{SW}$ in Figures 11 and 12, respectively), in which two hydroxyl groups (O^3H and O^5H) are attached to the C^4 atom of the peptide bond. From $\mathbf{I}_{WT}$, the generation of the $\mathbf{II}_{WT}$ intermediate is endothermic by 15.9 kcal/mol. However, for the SW-substrate the creation of this intermediate ($\mathbf{II}_{SW}$) is more favorable by 7.7 kcal/mol, i.e., 8.2 kcal/mol from $\mathbf{I}_{SW}$. In our previous study also the formation of the gem-diol intermediate for the cleavage of the Val-Ile and Ala-Thr peptide bonds by PS1 were calculated to be 6.2 and 17.4 kcal/mol, respectively.[42] In addition, the formation of this intermediate in the mechanism of HIV-1 protease for the cleavage of the Gly-Thr peptide bond is calculated to be endothermic by 10−12 kcal/mol.[40] The creation of the oxyanion species [$C(OH)(O^-)$] in this step was found to be prohibitively high (>35.0 kcal/mol) for both the substrates. The high endothermicity of this intermediate is in agreement with the previous studies on PS1[42] and HIV-1 protease.[87] In both $\mathbf{II}_{WT}$ and $\mathbf{II}_{SW}$, C^4-O^3H and C^4-O^5H groups interact through strong hydrogen bonding with the side chain ($C-O^1$) of Asp32 (O^3H-O^7 = 1.58 Å and O^5H-O^1 = 1.75 Å in $\mathbf{II}_{WT}$ (Figure 11) and O^3H-O^7 = 1.59 Å and O^5H-O^1 = 1.68 Å in $\mathbf{II}_{SW}$ (Figure 12). In addition, Asp228 forms a hydrogen bond with the hydroxyl ($-O^3H$) group (O^2H-O^3 = 1.52 Å) group in $\mathbf{II}_{WT}$ that is 0.24 Å shorter than the corresponding bond in $\mathbf{II}_{SW}$. In $\mathbf{II}_{WT}$ and $\mathbf{II}_{SW}$, the protonation states of Asp32 and Asp228 are now interchanged; that is, the former is in unprotonated form, while the latter is protonated that prepares the enzyme for the cleavage of the peptide bond in the next step.

These results explicitly exhibit that the formation of the gem-diol intermediate for the SW-substrate is energetically more favorable.

Cleavage of the Peptide Bond. In this step, both Asp32 and Asp228 interchange their roles from the previous step. From $\mathbf{II}_{WT}$, the Asp228 residue, which acted as a base and became protonated in the first step, now acts as an acid and donates its previously acquired proton to the backbone amine ($-N^6H$) group of Asp3. This step proceeds with the simultaneous abstraction of a proton bound to the O^3 atom of the gem-diol species by Asp32. This double proton exchange results in the cleavage of the peptide bond and the separated carboxyl ($-C^4O^3O^5H$) and amine ($-N^6H_2$) groups are formed.

From $\mathbf{II}_{WT}$, this process occurs with a very small barrier, i.e., 1.2 kcal/mol. Since this step is followed by a step that is endothermic by 15.9 kcal/mol, the overall barrier for this process becomes 17.1 kcal/mol from $\mathbf{I}_{WT}$. The fully optimized transition states ($\mathbf{TSII}_{WT}/\mathbf{TSII}_{SW}$) are shown in Figure 11 and Figure 12, respectively. The O^2-H = 1.75 Å, N^6-H = 1.07 Å, C^4-N^6 = 1.69 Å, O^5-H = 1.38 Å, and O^1-H = 1.11 Å bond distances for $\mathbf{TSII}_{WT}$ and the O^2-H = 1.30 Å, N^6-H = 1.28 Å, C^4-N^6 = 1. 53 Å, O^5-H = 1.19 Å, and O^1-H = 1.46 Å bond distances for $\mathbf{TSII}_{SW}$ indicate that these processes are concerted. The computed barrier of this step for the WT substrate is 7.3 (10.3) kcal/mol higher than the one computed for the SW substrate. The origin of this difference is likely to be the significant structural differences observed in the $\mathbf{II}_{WT}/\mathbf{II}_{SW} \rightarrow \mathbf{TSII}_{WT}/\mathbf{TSII}_{SW}$ transformations. The peptide bond distance in $\mathbf{TSII}_{WT}$ is substantially more elongated (by 0.16 Å) than in $\mathbf{TSII}_{SW}$. The critical O^2-H-O^3 and O^5-H-O^1 bond distances in $\mathbf{II}_{WT}$ are also 0.24 and 0.07 Å shorter and longer, respectively, than in $\mathbf{II}_{SW}$. These differences indicate that during the course of reaction the transfers of the protons bound to the O^2 and O^5 atoms from $\mathbf{II}_{WT}$ cost more than the corresponding transfers from $\mathbf{II}_{SW}$. In both the cases, the connections between the fully optimized transition state ($\mathbf{TSII}_{WT}$ and $\mathbf{TSII}_{SW}$) and the gem-diol intermediate were confirmed by using 30 steps intrinsic reaction coordinate (IRC) calculations in the backward direction followed by the full optimizations. From $\mathbf{I}_{WT}$, the hydrolysis of the Met2-Asp3 peptide bond leading to the formation of the separated -Met-COOH and -Asp-NH_2 terminals ($\mathbf{III}_{WT}$) is exothermic by 5.7 (5.2) kcal/mol. The generation of the final product ($\mathbf{III}_{SW}$) in the cleavage of the Leu2-Asp3 bond of the SW substrate also occur with the similar exothermicity, i.e., 5.2 (2.8) kcal/mol from $\mathbf{I}_{SW}$. At the end of the reaction, the enzyme returns back to its original form, in which Asp32 and Asp228 exist in protonated and unprotonated forms, respectively.

These calculations show that the cleavage of the SW-substrate is energetically more favorable and in line with the experimental observation that BACE1 cleaves the SW substrate 60 times more efficiently than the WT substrate.

SUMMARY AND CONCLUSIONS

In this combined MD simulation and DFT study, the process of flap closing upon the binding of the WT and SW substrates in the open flap conformation of BACE1 and their cleavage mechanisms have been investigated. A good agreement between the key structural features of the equilibrated and X-ray (PDB ID: 2QMG) structures of the SC6 inhibitor bound BACE1-SC6 complex validates the accuracy of these simulations.

Upon the binding of the WT and SW substrates at the active site, the flap of the enzyme closes around 3 ns and water molecules play an important role in this process. As suggested previously,[27] the two catalytic water molecules formed the H-boding network at the active site involving the Asp32, Ser35, Asn37, Tyr71, and Asp228 residues of the enzyme. In a site-directed mutagenesis study,[79] electrostatic interactions between the Glu (P4) and Arg307 were reported to enhance the catalytic efficiency of BACE1. In the BACE1-WT simulation, this interaction is lost and Glu (P4) associates with the Lys (P2) residue of the substrate. The loss of the Glu (P4)-Arg307 interaction may contribute to the reduced activity of the enzyme toward the WT-substrate.[28] A comparison between the key interatomic distances (C^α(Thr72)−C^β(Asp32), C^α(Thr72)−C^α(Thr329), and OG1-(Thr72)−NH1(Arg235)) and the volume of the active site computed from the BACE1-WT and BACE1-SW simulations show that, in comparison to the WT-substrate, the flap is more closed and the active site is more contracted upon the binding of the SW-substrate. The hydrophobic interactions of the SW-substrate with the active site are also observed to be different than the WT-substrate and the former forms ca. 2 times (8−10)

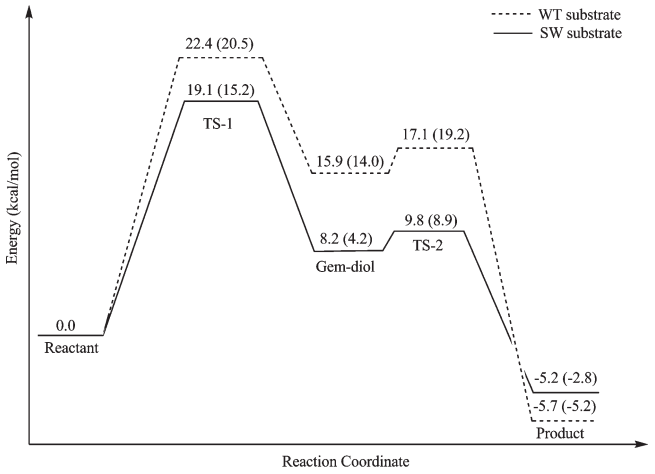

Figure 13. Potential energy diagrams for the cleavage of the Met2-Asp3 peptide bond of the WT-substrate (dotted line) and the Leu2-Asp3 bond of the WT-substrate (solid line) catalyzed by BACE1.

more hydrogen bonds than the later. The electrostatic binding energy of −6.5 kcal/mol for the SW-substrate calculated using APBS is 1.9 kcal/mol greater than the corresponding energy for the WT-substrate. Upon the binding of the SW-substrate, structures and positions of the inserts A, D, and F and the 10s loop of the enzyme are also substantially different than the ones observed for the WT-substrate. All the results obtained from the MD simulations indicate that, in comparison to the WT-substrate, BACE1 exhibits greater affinity for the SW-substrate and positions it in a more reactive conformation.

In the next step, the most representative structures derived from the BACE1-WT and BACE1-SW simulations were utilized to develop pruned models of the enzyme−substrate complexes to investigate cleavage mechanisms of both the substrates. The general acid/base mechanism of the hydrolytic cleavage of the Met2-Asp3 and Leu2-Asp3 peptide bond of the WT- and SW-substrate, respectively, by BACE1 proceeds through the following two steps: (1) generation of the gem-diol intermediate and (2) cleavage of the peptide bond. The potential energy surface (PES) diagrams for these reactions are shown in Figure 13. For both the substrates, the formation of the gem-diol intermediate in the first step was found to be the rate-determining step of the entire mechanism. With the barrier of 22.4 kcal/mol, this process for the WT-substrate is 3.3 kcal/mol higher than the SW-substrate (19.1 kcal/mol). The structural differences in the microenvironment of the active site play a critical role in lowering of the barrier for the SW-substrate. The computed barrier is in good agreement with the experimentally measured barrier of ca. 18.00 kcal/mol for the WT-substrate.[48] The creation of the gem-diol intermediate for the SW-substrate is 7.7 kcal/mol more favorable (8.2 kcal/mol from $\mathbf{I_{SW}}$) than for the WT-substrate. The overall barrier for the collapse of the gem-diol intermediate ($\mathbf{II_{WT}}$) for the WT-substrate is 7.3 (10.3) kcal/mol higher than the one for the SW-substrate (8.2 (4.2) kcal/mol from $\mathbf{I_{SW}}$). However, the exothermicities of the separated carboxyl (−COOH) and amine ($-NH_2$) terminals in the final product for both the substrates are quite similar, i.e., 5.7 (5.2) for $\mathbf{III_{WT}}$ and 5.2 (2.8) for $\mathbf{III_{SW}}$. The computed energetics show that BACE1 is more efficient in cleaving the SW substrate and in accord with the experimental observation that the cleavage of the WT-substrate is 60 times less efficient than the SW-substrate.[28,29]

The results presented in this study will enhance our understanding of the substrate specificity and cleavage mechanism of this critical enzyme and advance scientific efforts toward its utilization as a therapeutic intervention for Alzheimer's disease.

■ ASSOCIATED CONTENT

Supporting Information. (a) Complete reference;[58] (b) details of the APBS calculations; (c) Figures S1−S6; (d) Tables S1−S7: Cartesian coordinates (in Å) of all the optimized structures for the WT-substrate; Tables S8−S14: Cartesian coordinates (in Å) of all the optimized structures for the SW-substrate. This material is available free of charge via the Internet at http://pubs.acs.org.

■ AUTHOR INFORMATION

Corresponding Author
*E-mail: rpr@miami.edu. Tel: 305-284-9372. Fax: 305-284-4571.

Funding Sources
A funding grant (DOH Grant 08KN-11) to R.P. from the James and Esther King Biomedical Research Program of the Florida State Health Department is acknowledged.

■ ACKNOWLEDGMENT

Computational resources from the Center for Computational Science (CCS) at the University of Miami are greatly appreciated.

■ ABBREVIATIONS

BACE1, β-Secretase; Aβ, amyloid beta; AD, Alzheimer's disease; MD, molecular dynamics; APP, amyloid precursor protein; PDB, Protein Data Bank; OPLS, Optimized Potentials for Liquid Simulations.

■ REFERENCES

(1) Northrop, D. B. (2001) Follow the Protons: A Low-Barrier Hydrogen Bond Unifies the Mechanisms of the Aspartic Proteases. *Acc. Chem. Res. 34*, 790–797.

(2) Davies, D. R. (1990) The Structure and Function of the Aspartic Proteinases. *Annu. Rev. Biophys. Biophys. Chem. 19*, 189–215.

(3) Miller, M., Jaskolski, M., Rao, J. K. M., Leis, J., and Wlodawer, A. (1989) Crystal structure of a retroviral protease proves relationship to aspartic protease family. *Nature 337*, 576–579.

(4) Navia, M. A., Fitzgerald, P. M. D., McKeever, B. M., Leu, C.-T., Heimbach, J. C., Herber, W. K., Sigal, I. S., Darke, P. L., and Springer, J. P. (1989) Three-dimensional structure of aspartyl protease from human immunodeficiency virus HIV-1. *Nature 337*, 615–620.

(5) Rawlings, N. D., and Barrett, A. J. (1995) [7] Families of aspartic peptidases, and those of unknown catalytic mechanism. In *Methods in Enzymology* (Alan, J. B., Ed.), pp 105−120, Academic Press, New York.

(6) Dunn, B. M. (2002) Structure and Mechanism of the Pepsin-Like Family of Aspartic Peptidases. *Chem. Rev. 102*, 4431–4458.

(7) Tang, J., James, M. N. G., Hsu, I. N., Jenkins, J. A., and Blundell, T. L. (1978) Structural evidence for gene duplication in the evolution of the acid proteases. *Nature 271*, 618–621.

(8) Blundell, T. L., and Srinivasan, N. (1996) Symmetry, stability, and dynamics of multidomain and multicomponent protein systems. *Proc. Natl. Acad. Sci. U.S.A. 93*, 14243–14248.

(9) Marcinkeviciene, J., Luo, Y., Graciani, N. R., Combs, A. P., and Copeland, R. A. (2001) Mechanism of Inhibition of β-Site Amyloid Precursor Protein-cleaving Enzyme (BACE) by a Statine-based Peptide. *J. Biol. Chem. 276*, 23790–23794.

(10) Amyloid Proteins (2005) in *The Beta Sheet Conformation and Disease* (Sipe, J. D., Ed.) Vol. 2, Wiley-VCH, New York.

(11) Yan, R., Bienkowski, M. E., Shuck, M. E., Miao, H., Tory, M. C., Pauley, A. M., Brashler, J. R., Stratman, N. C., Mathews, W. R., Buhl, A. E., Carter, D. B., Tomasselli, A. G., Parodi, L. A., Heinrikson, R. L., and Gurney, M. E. (1999) Membrane-anchored aspartyl protease with Alzheimer's disease β-secretase activity. *Nature 402*, 533–537.

(12) Pillot, T., Drouet, B., Queille, S., Labeur, C., Vandekerckhove, J., Rosseneu, M., Pincon-Raymond, M., and Chambaz, J. (1999) The Nonfibrillar Amyloid β-Peptide Induces Apoptotic Neuronal Cell Death. Involvement of Its C-Terminal Fusogenic Domain. *J. Neurochem. 73*, 1626–1634.

(13) Suo, Z. M., Humphrey, J., Kundtz, A., Sethi, F., Placzek, A., Crawford, F., and Mullan, M. (1998) Soluble Alzheimers β-amyloid constricts the cerebral vasculature in vivo. *Neurosci. Lett. 257*, 77–80.

(14) Vassar, R., Bennett, B. D., Babu-Khan, S., Kahn, S., Mendiaz, E. A., Denis, P., Teplow, D. B., Ross, S., Amarante, P., Loeloff, R., Luo, Y., Fisher, S., Fuller, J., Edenson, S., Lile, J., Jarosinski, M. A., Biere, A. L., Curran, E., Burgess, T., Louis, J.-C., Collins, F., Treanor, J., Rogers, G., and Citron, M. (1999) β-Secretase Cleavage of Alzheimer's Amyloid Precursor Protein by the Transmembrane Aspartic Protease BACE. *Science 286*, 735–741.

(15) Sinha, S., Anderson, J. P., Barbour, R., Basi, G. S., Caccavello, R., Davis, D., Doan, M., Dovey, H. F., Frigon, N., Hong, J., Jacobson-Croak, K., Jewett, N., Keim, P., Knops, J., Lieberburg, I., Power, M., Tan, H., Tatsuno, G., Tung, J., Schenk, D., Seubert, P., Suomensaari, S. M., Wang, S., Walker, D., Zhao, J., McConlog, L., and John, V. (1999) Purification and cloning of amyloid precursor protein β-secretase from human brain. *Nature 402*, 537–540.

(16) Stockley, J., and O'Neill, C. (2008) Understanding BACE1: essential protease for amyloid-β production in Alzheimer's disease. *Cell. Mol. Life Sci. 65*, 3265–3289.

(17) Strooper, B. D. (2010) Proteases and Proteolysis in Alzheimer Disease: A Multifactorial View on the Disease Process. *Physiol. Rev. 90*, 465–494.

(18) Cai, H., Wang, Y., McCarthy, D., Wen, H., Borchelt, D. R., and Price, D. L. (2001) BACE1 is the major beta-secretase for generation of Aβ peptides by neurons. *Nature Neurosci. 4*, 233–234.

(19) Luo, Y., Bolon, B., Kahn, S., Bennett, B. D., Babu-Khan, S., Denis, P., Fan, W., Kha, H., Zhang, J., Gong, Y., Martin, L., Louis, J.-C., Yan, Q., Richards, W. G., Martin Citron, M., and Vassar, R. (2001) Mice deficient in BACE1, the Alzheimer's β-secretase, have normal phenotype and abolished β-amyloid generation. *Nature Neurosci. 4*, 231–232.

(20) Shimizu, H., Tosaki, A., Kaneko, K., Hisano, T., Sakurai, T., and Nukina, N. (2008) Crystal Structure of an Active Form of BACE1, an Enzyme Responsible for Amyloid β Protein Production. *Mol. Cell. Biol. 28*, 3663–3671.

(21) Hong, L., Koelsch, G., Lin, X., Wu, S., Terzyan, S., Ghosh, A. K., Zhang, X. C., and Tang, J. (2000) Structure of the Protease Domain of Memapsin 2 (β-Secretase) Complexed with Inhibitor. *Science 290*, 150–153.

(22) Patel, S., Vuillard, L., Cleasby, A., Murray, C. W., and Yon, J. (2004) Apo and Inhibitor Complex Structures of BACE (β-secretase). *J. Mol. Biol. 343*, 407–416.

(23) Hong, L., Turner, R. T., III, Koelsch, G., Shin, G., Ghosh, A. K., and Tang, J. (2002) Crystal structure of memapsin 2 (β-secretase) complexed with an inhibitor OM00−3. *Biochemistry 41*, 10963–10967.

(24) Hong, L., and Tang, J. (2004) Flap position of free memapsin 2 (β-Secretase), a model for flap opening in aspartic protease catalysis. *Biochemistry 43*, 4689–4695.

(25) Xiong, B., Huang, X., Shen, L., Shen, J., Luo, X., Shen, X., Jiang, H., and Chen, K. (2004) Conformational flexibility of β-secretase: molecular dynamics simulation and essential dynamics analysis. *Acta. Pharmacol. Sin. 25*, 705–713.

(26) Gorfe, A. A., and Caflisch, A. (2005) Functional Plasticity in the Substrate Binding Site of β-Secretase. *Structure 13*, 1487–1498.

(27) Andreeva, N. S., and Rumsh, L. D. (2001) Analysis of crystal structures of aspartyl protinases: On the role of amino acid residues adjacent to the catalytic site of pepsin-like enzymes. *Protein Sci. 10*, 2439–2450.

(28) Citron, M., Diehl, T. S., Gordon, G., Biere, A. L., Seubert, P., and Selkoe, D. J. (1996) Evidence that the 42- and 40-amino acid forms of amyloid β protein are generated from the β-amyloid precursor protein by different protease activities. *Proc. Natl. Acad. Sci. U.S.A. 93*, 13170–13175.

(29) Cai, X. D., Golde, T. E., and Younkin, S. G. (1993) Release of excess amyloid beta protein from a mutant amyloid beta protein precursor. *Science 259*, 514–516.

(30) Grüninger-Leitch, F., Schlatter, D., Küng, E., Nelböck, P., and Döbeli, H. (2002) Substrate and Inhibitor Profile of BACE (β-Secretase) and Comparison with Other Mammalian Aspartic Proteases. *J. Biol. Chem. 277*, 4687–4693.

(31) Wolfe, M. S., Xia, W., Moore, C. L., Leatherwood, D. D., Ostaszewski, B., Rahmati, T., Donkor, I. O., and Selkoe, D. J. (1999) Peptidomimetic Probes and Molecular Modeling Suggest That Alzheimer's γ-Secretase Is an Intramembrane-Cleaving Aspartyl Protease. *Biochemistry 38*, 4720–4727.

(32) Coates, L., Erskine, P. T., Mall, S., Gill, R., Wood, S. P., Myles, D. A., and Cooper, J. B. (2006) X-ray, neutron and NMR studies of teh catalytic mechanism of aspartic proteinases. *Eur. Biophys. J. 35*, 559–566.

(33) Coates, L., Tuan, H.-F., Tomanicek, S., Kovalevsky, A., Mustyakimov, M., Erskine, P. T., and Cooper, J. B. (2008) The catalytic mechanism of an aspartic proteinase explored with neutron and x-ray diffraction. *J. Am. Chem. Soc. 130*, 7235–7237.

(34) Rajamani, R., and Reynolds, C. H. (2004) Modeling the Protonation States of the Catalytic Aspartates in β-Secretase. *J. Med. Chem. 47*, 5159–5166.

(35) Yu, N., Hayik, S. A., Wang, B., Liao, N., Reynolds, C. H., and Merz, K. M. (2006) Assigning the Protonation States of the Key Aspartates in β-Secretase Using QM/MM X-ray Structure Refinement. *J. Chem. Theory Comput. 2*, 1057–1069.

(36) Suguna, K., Padlan, E. A., Smith, C. W., Carlson, W. D., and Davies, D. R. (1987) Binding of a reduced peptide inhibitor to the aspartic proteinase from Rhizopus chinensis: implications for a mechanism of action. *Proc. Natl. Acad. Sci. U.S.A. 84*, 7009–7013.

(37) Bjelic, S., and Åqvist, J. (2006) Catalysis and linear free energy relationship in aspartic proteases. *Biochemistry 45*, 7709–7723.

(38) Cascella, M., Micheletti, C., Rothlisberger, U., and Carloni, P. (2005) Evolutionarily Conserved Functional Mechanics across Pepsin-like and Retroviral Aspartic Proteases. *J. Am. Chem. Soc. 127*, 3734–3742.

(39) Chatfield, D., Eurenius, C. P., Brooks, K., and Bernard, R. (1998) HIV-1 protease cleavage mechanism: A theoretical investigation based on classical MD simulation and reaction path calculations using a hybrid QM/MM potential. *J. Mol. Struct.: THEOCHEM 423*, 79–92.

(40) Piana, S., Bucher, D., Carloni, P., and Rothlisberger, U. (2004) Reaction Mechanism of HIV-1 Protease by Hybrid Car-Parrinello/Classical MD Simulations. *J. Phys. Chem. B 108*, 11139–11149.

(41) Trylska, J., Grochowski, P., and McCammon, J. A. (2004) The role of hydrogen bonding in the enzymatic reaction catalyzed by HIV-1 protease. *Protein Sci. 13*, 513–528.

(42) Singh, R., Barman, A., and Prabhakar, R. (2009) Computational Insights into Aspartyl Protease Activity of Presenilin 1 (PS1) Generating Alzheimer Amyloid β-Peptides (Aβ40 and Aβ42). *J. Phys. Chem. B 113*, 2990–2999.

(43) Strajbl, M., Florian, J., and Warshel, A. (2000) Ab Initio Evaluation of the Potential Surface for General Base- Catalyzed Methanolysis of Formamide: A Reference Solution Reaction for Studies of Serine Proteases. *J. Am. Chem. Soc. 122*, 5354–5366.

(44) Wu, Z., Ban, F., and Boyd, R. J. (2003) Modeling the reaction mechanisms of the amide hydrolysis in an N-(o--Carboxybenzoyl)-L-amino acid. *J. Am. Chem. Soc. 125*, 6994–7000.

(45) Park, H., Suh, J., and Lee, S. (2000) Ab initio studies on the catalytic mechanism of aspartic proteinases: nucleophilic versus general acid/base mechanism. *J. Am. Chem. Soc. 122*, 3901–3908.

(46) Antonczak, S., Ruiz-Lopez, M. F., and Rivail, J. L. (1994) Ab initio analysis of water-assisted reaction mechanisms in amide hydrolysis. *J. Am. Chem. Soc. 116*, 3912–3921.

(47) Piana, S., Parrinello, M., and Carloni, P. (2002) Role of conformational fluctuations in the enzymatic reaction of HIV-1 protease. *J. Mol. Biol. 319*, 567–583.

(48) Lin, X., Koelsch, G., Wu, S., Downs, D., Dashti, A., and Tang, J. (2000) Human aspartic protease memapsin 2 cleaves the β-amyloid precursor protein. *Proc. Natl. Acad. Sci. U.S.A. 97*, 1456–1460.

(49) Iserloh, U., Pan, J., Stamford, A. W., Kennedy, M. E., Zhang, Q., Zhang, L., Parker, E. M., McHugh, N. A., Favreau, L., Strickland, C., and Voigt, J. (2008) Discovery of an orally efficaceous 4-phenoxypyrrolidine-based BACE-1 inhibitor. *Bioorg. Med. Chem. Lett. 18*, 418–422.

(50) Berendsen, H. J. C., van der Spoel, D., and van Drunen, D. (1995) GROMACS: A message-passing parallel molecular dynamics implementation. *Comput. Phys. Commun. 91*, 43–56.

(51) Lindahl, E., Hess, B., and van der Spoel, D. (2001) GROMACS 3.0: a package for molecular simulation and trajectory analysis. *J. Mol. Model. 7*, 306–317.

(52) Jorgensen, W. L., and Tirado-Rives, J. (1988) The OPLS [optimized potentials for liquid simulations] potential functions for proteins, energy minimizations for crystals of cyclic peptides and crambin. *J. Am. Chem. Soc. 110*, 1657–1666.

(53) Kaminski, G. A., Friesner, R. A., Tirado-Rives, J., and Jorgensen, W. L. (2001) Evaluation and reparametrization of the OPLS-AA force field for proteins via comparison with accurate quantum chemical calculations on peptides. *J. Phys. Chem. B 105*, 6474–6487.

(54) Ribeiro, A. A. S. T., Horta, B. A. C., and de Alencastro, R. B. (2008) MKTOP: a Program for automatic construction of molecular topologies. *J. Braz. Chem. Soc. 19*, 1433–1435.

(55) Brenneman, C. M., and Wiberg, K. B. (1990) Determining atom-centered monopoles from molecular electrostatic potentials. The need for high sampling density in formamide conformational analysis. *J. Comput. Chem. 11*, 361–373.

(56) Becke, A. D. (1988) (1988) Density-functional exchange-energy approximation with correct asymptotic behavior. *Phys. Rev. A 38*, 3098–3100.

(57) Lee, C., Yang, W., and Parr, R. G. (1988) Development of the Colle-Salvetti correlation energy formula into a functional of the electron density. *Phys. Rev. B 37*, 785–789.

(58) Frisch, M. J., (2009) *Gaussian 09*, Revision A.1 ed., Gaussian Inc., Wallingford, CT.

(59) Jorgensen, W. L., Chandrasekhar, J., Madura, J. D., Impey, R. W., and Klein, M. L. (1983) Comparison of simple potential functions for simulating liquid water. *J. Chem. Phys. 79*, 926–935.

(60) Miyamoto, S., and Kollman, P. A. (1992) SETTLE: An analytical version of the SHAKE and RATTLE algorithms for rigid water models. *J. Comput. Chem. 13*, 952–062.

(61) Hess, B., Bekker, H., Berendsen, H. J. C., and Fraaije, J. G. E. M. (1997) LINCS: A linear constraint solver for molecular simulations. *J. Comput. Chem. 18*, 1463–1472.

(62) Darden, T. A., York, D., and Pedersen, L. (1993) Particle mesh Ewald: An N·log(N) method for Ewald sums in large systems. *J. Chem. Phys. 98*, 10089–10092.

(63) York, D. M., Wlodawer, A., Pedersen, L. G., and Darden, T. A. (1994) Atomic-Level Accuracy in Simulations of Large Protein Crystals. *Proc. Natl. Acad. Sci. U.S.A. 91*, 8715–8718.

(64) Krieger, E., and Vriend, G. (2002) Models@home: distributed computing in bioinformatics using a screensaver based approach. *Bioinformatics 18*, 315–318.

(65) DeLano, W. L. (2002) *The PyMOL Molecular Graphics System*, DeLano Scientific, Palo Alto, CA.

(66) Humphrey, W., Dalke, A., and Schulten, K. (1996) VMD - Visual Molecular Dynamics. *J. Mol. Graphics 14*, 33–38.

(67) Sharp, K. A., and Honig, B. (1990) Calculating total electrostatic energies with the nonlinear Poisson-Boltzmann equation. *J. Phys. Chem. 94*, 7684–7692.

(68) Baker, N., Holst, M., and Wang, F. (2000) Adaptive multilevel finite element solution of the Poisson-Boltzmann equation II. Refinement at solvent-accessible surfaces in biomolecular systems. *J. Comput. Chem. 21*, 1343–1352.

(69) Baker, N. A., Sept, D., Joseph, S., Holst, M. J., and McCammon, J. A. (2001) Electrostatics of nanosystems: Application to microtubules and the ribosome. *Proc. Natl. Acad. Sci. U.S.A. 98*, 10037–10041.

(70) Bowers, K. J. C., E., Xu, H., Dror, R. O., Eastwood, M. P., Gregersen, B. A., Klepeis, J. L., Kolossváry, I., Moraes, M. A., Sacerdoti, F. D., Salmon, J. K., Shan, Y., and Shaw, D. E. (2006) Scalable Algorithms for Molecular Dynamics Simulations on Commodity Clusters in *Proceedings of the ACM/IEEE Conference on Supercomputing (SC06)*, Tampa, FL.

(71) Prabhakar, R., Morokuma, K., and Musaev, D. G. (2006) Peroxinitrite reductase activity of selenoprotein glutathione peroxidase (GPx): A density functional study. *Biochemistry 45*, 6967–6977.

(72) Siegbahn, P. E. M., and Blomberg, M. R. A. (2000) Transition metal systems in biochemistry studied by high-accuracy quantum chemical methods. *Chem. Rev. 100*, 421–437.

(73) Himo, F., and Siegbahn, P. E. M. (2003) Quantum chemical studies of radical-containing enzymes. *Chem. Rev. 103*, 2421–2456.

(74) Becke, A. D. J. (1993) Density-functional thermochemistry. III. The role of exact exchange. *Chem. Phys. 98*, 5648–5652.

(75) Noodleman, L., Lovell, T., Han, W. G., Li, J., and Himo, F. (2004) Quantum Chemical Studies of Intermediates and Reaction Pathways in Selected Enzymes and Catalytic Synthetic Systems. *Chem. Rev. 104*, 459–508.

(76) Cances, E., Mennucci, B., and Tomasi, J. (1997) A new integral equation formalism for the polarizable continuum model: theoretical background and applications to isotropic and anisotropic dielectrics. *J. Chem. Phys. 107*, 3032–3041.

(77) SiteMap. (2009) version 2.3 ed., Schrödinger LLC, New York.

(78) Turner, R. T., Hong, L., Koelsch, G., Ghosh, A. K., and Tang, J. (2004) Structural locations and functional roles of new subsites S5, S6, and S7 in memapsin 2 (β-Secretase). *Biochemistry 44*, 105–112.

(79) Turner, R. T., Koelsch, G., Hong, L., Castenheira, P., Ghosh, A., and Tang, J. (2001) Subsite specificity of memapsin 2 (β-Secretase): implications for inhibitor design. *Biochemistry 40*, 10001–10006.

(80) Siegbahn, P. E. M. (2003) Mechanisms of metalloenzymes studied by quantum chemical methods. *Q. Rev. Biophys. 36*, 91–145.

(81) Siegbahn, P. E. M. (2006) The performance of hybrid DFT for mechanism involving transition metal complexes in enzymes. *J. Biol. Inorg. Chem. 11*, 695–701.

(82) Shaik, S., Kumar, D., de Visser, S. P., Altun, A., and Thiel, W. (2005) Theoretical Perspective on the Structure and Mechanism of Cytochrome P450 Enzymes. *Chem. Rev. 105*, 2279–2328.

(83) Prabhakar, R., and Siegbahn, P. E. M. (2004) DFT study of the Mechanism for the biogenesis of cofactor topaquinone (TPQ) in Copper Amine Oxidases (CAOs). *J. Am. Chem. Soc. 107*, 3944–3953.

(84) Bora, R. P., Barman, A., Zhu, X., Ozbil, M., and Prabhakar, R. (2010) Which One Among Aspartyl Protease, Metallopeptidase, and Artificial Metallopeptidase is the Most Efficient Catalyst in Peptide Hydrolysis?. *J. Phys. Chem. B 114*, 10860–10875.

(85) Zhang, Y., Kua, J., and McCammon, J. A. (2003) Influence of Structural Fluctuation on Enzyme Reaction Energy Barriers in Combined Quantum Mechanical/Molecular Mechanical Studies. *J. Phys. Chem. B 107*, 4459–4463.

(86) Cui, Q., and Karplus, M. (2002) Quantum Mechanics/Molecular Mechanics Studies of Triosephosphate Isomerase-Catalyzed Reactions: Effect of Geometry and Tunneling on Proton-Transfer Rate Constants. *J. Am. Chem. Soc. 124*, 3093–3124.

(87) Carnevale, V., Raugei, S., Piana, S., and Carloni, P. (2008) On the nature of the reaction intermediate in the HIV-1 protease: a quantum chemical study. *Comput. Phys. Commun. 179*, 120–123.